Designing structurally optimal composites using plant stem material and comparing to their natural counterpart.

Rohit Gupta, Sumit Basu

July 10, 2019

Contents

List of Figures

1 Introduction

Functionally graded composites (FGCs) are generally designed with certain properties in focus. Two or more materials with contrasting and complementing properties are combined in a number of ways obtain a composite with unique combination of characteristics. Unlike man-made composites, natural materials (most of which can be classified as composites) are far more complex in structure and organisation and superior in properties. Natural material typically shows a hierarchical organisation of an array of simple chemical[25] . Such organisation can be seen at macroscale and all the way down to nanoscale. Creating structures with similar organisation is generally the goal behind studying functionally graded composites.

Plant and tree stems are natural structure with a unique combination of strength and light weight. Natural material like bamboo are being tested as replacement for concrete reinforcement[5]. These structure have gone through a lot of iteration during the process of evolution. All natural materials have been selected to be the best in their respective environment given the availability of resources[19]. Most of the natural material perform better then man-made materials on performance matrices such as $\frac{E^{1/2}}{\rho}$ etc.[2][7]. Mwaikambo et. al. [17] showed that there is strong relationship between the physical and mechanical properties of the stem and their fine microstructure.

Silva et. al. [23] have modelled bamboo as a functionally graded material which consists of lignin-carbohydrate complex and long cellulose fibres. Youssefian et. al. [26] showed that fibres are mainly responsible for the strength while the ligin matrix captures air making the structure lighter.

For studying plant stems, we have chosen bamboo as the candidate. Our approach is gradual meaning we will start with 1D simulation and go on to compare the 3D structure of bamboo with an equivalent but optimal functionally graded material composed of material with similar mechanical properties as that of the consituents of bamboo. In this thesis, however, 1D simulations and code for obtaining optimal 2D cellular structures will be discussed.

On a macro level bamboo has an asymmetric distribution of material[9]. The aerial distribution of material across the cross-section can modelled in 1D. This is modelled as a nonlinear optimization problem [24] as discussed in the first chapter. For obtaining 2D models optimum FGCs, topology optimization[3] with homogenization has been used. Sigmund et. al. [22] tackled the problems of numerical instabilites associated with topology optimization problem such as mesh-dependent solution, checkboard pattern in the topology etc by developing mesh independency filters. Lazarov et. al. [14] studied a number of such filters. Papanicolau et. al. [20] and Sanchez et. al. [21] developed the theory of a homogenization. This is based on the asymptotic expansion of the system response. Bendose et. al. [4] developed the method of applying homogenization techniques to the problem of topology optimization at multi-scale. Zhang et. al. [27] proposed a design element concept and compared with approach of asymptotic homogenization. Hassani et. al. [10] discussed the periodic boundary condition needed for the process of homogenization.

There have been many application of this method of two scale topology optimization [13][11][18]. This method of optimization particularly suit our problem. Since the microstructure of bamboo consists of parenchyma cell and long fibres, i.e., a periodic cellular microstructure. This optimization approach is best suited for periodic structures.

2 1D Simulation

Bamboo is a natural composite which is composed of fibers embedded in a matrix of parenchyma cells. Bamboo fibers are mainly composed of cellulose, hemicellulose and lignin.[17] Fibers are spread out across the cross-section in a graded manner with higher density towards the periphery. Also, the size of parenchyma cells decreases along the radially outward direction as the air content reduces. This results in axisymmetric areal density variation in the radial direction (fig. 1).
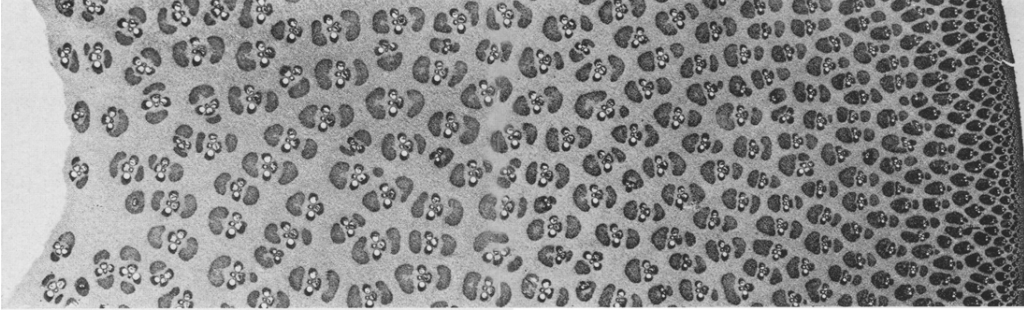
Figure 1: Sector of cross-section showing distribution of fibre bundles. [8]

This can be modeled as the distribution of two materials, and air (captured in parenchyma cells). First material being the denser and stiffer fibers and second material being the parenchyma cellular material excluding air. The properties of fibers and parenchyma are taken from [15][17].

Bamboo, like any other living organism, is a result of an evolutionary process. Survival of the fittest means that bamboo species is nature's best solution for some natural condition lead to the existence of bamboo. Bamboo grows tall up to 20m to rise above the other competing plantation. With such a slender structure, bending load due to high-speed tropical winds are a significant constraint which the evolution had overcome. Bamboo has a very high specific strength, which is also the desired attribute in industrial applications. It is desired to develop composites with high stiffness and lower weight.

2.1 Formulation

Therefore, we frame a constrained problem, optimizing the radial distribution of two material, with properties corresponding to that of fibers and parenchyma, in an annular cross-section composites. The objective function to optimize is specific strength subjected to the constraints of maximum stress and maximum bending moment. The dimensions of the composites are kept the same as in [15]. Also, the limits of max bending moment and stress are taken from [15]. The general problem formulation is written as

$$
\begin{aligned}
\underset{\chi}{\text{maximize}} \quad & strength(\chi) \\
\text{subject to} \quad & \sigma(r) \leq \sigma_{max} \qquad \forall r \in [r_i, r_o] \\
& M \leq M_{max}
\end{aligned}
$$

where, χ is the distribution of the two material in the domain whose inner radius is r_i and outer radius is r_o. σ is the stress in the longitudinal direction and M is the bending moment.

2.2 Implementation

Now, flexural rigidity is used as measure of strength which can be written as

$$EI(r) = \iint_R E(r)y^2 \, dA = \int_{r_1}^{r_2} \int_0^{2\pi} E(r)(r\sin\theta)^2(rdrd\theta)$$
$$= \pi \int_{r_1}^{r_2} E(r)r^3 dr \qquad \text{Integrating over } \theta \tag{1}$$
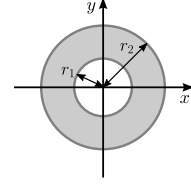
Figure 2: Annulus with inner radius r1 and outer radius r2

Therefore, specific flexural rigidity will be written as

$$strength(\chi) = \frac{EI}{\rho}$$
$$= \frac{\pi \sum_{r_i}^{r_o} E(r)r^3 \Delta r}{2\pi r \sum_{r_i}^{r_o} \rho(r)\Delta r}$$
$$= \frac{\sum_{r_i}^{r_o} E(r)r^3}{2\sum_{r_i}^{r_o} \rho(r)r} \tag{2}$$

where

$$E(r) = \chi_1(r)E_1 + \chi_2(r)E_2$$
$$\rho(r) = \chi_1(r)\rho_1 + \chi_2(r)\rho_2 \tag{3}$$

Here $\{E_1, \rho_1\}$ and $\{E_2, \rho_2\}$ are the material properties of the fibers and parenchyma respectively. χ_1 and χ_2 are the proportion of first and second material corresponding to fiber and parenchyma respectively.

Assuming small deformation, from Euler Bernoulli Beam Theory, we get strain ε_{xx} as

$$\varepsilon_{xx} = \frac{\Delta x' - \Delta x}{\Delta x}$$
$$= \frac{(R+y)\Delta\theta - R\Delta\theta}{R\Delta\theta}$$
$$= \frac{y}{R} \tag{4}$$

Therefore, using constitutive relation, we get σ_{xx} as

$$\sigma_{xx} = E\varepsilon_{xx} = \frac{E}{R}y \tag{5}$$

$$\sigma = \frac{E}{R}r\sin\theta \quad (\because y = r\sin\theta) \tag{6}$$
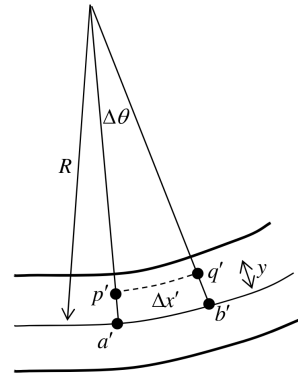
Figure 3: Beam deformation

Now, moment can be written as

$$M(x) = \int\int y \cdot \sigma(x,y) \cdot dy dz$$

$$M = \int_{r_i}^{r_o} \int_0^{2\pi} \sigma(r) r^2 sin\theta \, dr \, d\theta \qquad \text{For a particular } x$$

$$= \int_{r_i}^{r_o} \int_0^{2\pi} \frac{E(r) r sin\theta}{R} r^2 sin\theta \, dr \, d\theta \qquad \text{(From eqn (6))}$$

$$= \pi \int_{r_i}^{r_o} \frac{r^3 E(r)}{R} \, dr$$

(7)

2.3   Optimization Problem

Using (2), (6), (7), the optimization problem becomes

$$\max_{\chi} \quad \frac{\sum_{r_i}^{r_o} E(r) r^3}{\sum_{r_i}^{r_o} \rho(r) r}$$

$$s.t. \quad \frac{r E(r)}{R} \leq \sigma_{max} \quad \forall r \in [r_i, r_o]$$

$$\sum_{r_i}^{r_o} r^3 E(r) \leq \frac{M_{max} R}{\pi \Delta r}$$

(8)

2.4   Cell Size

For calculating parenchyma cell size, it is assumed that the cell thickness remains constant as we move from inner radius to the outer radius. The cell thickness has been determined from the dimensions given in Figure 4(a) in [16].

(a)   (b)
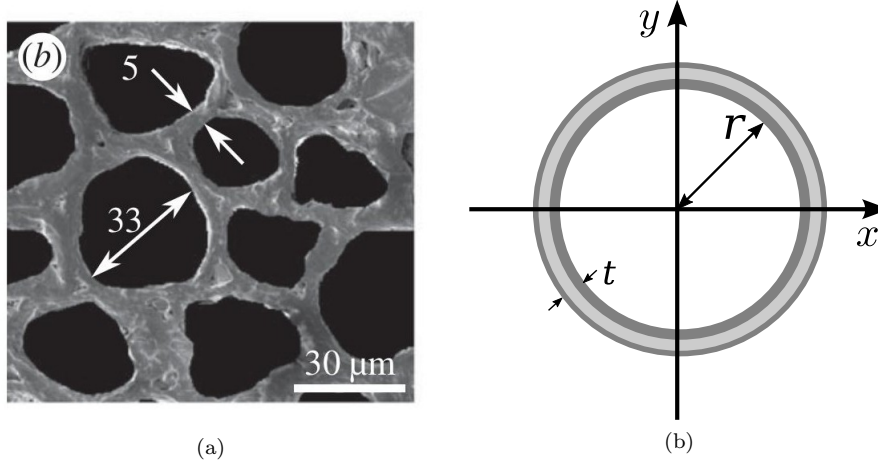
Figure 4: Cross-sectional micrograph showing the dimensions of typical parenchyma cell [16]

Parenchyma cells consists of cellular material and air packets. Assuming cell to be spherical, let v_a be the volume of air and v_p be the volume of cellular material. From fig. 4

$$v_a = \frac{4}{3}\pi r^3$$
$$v_p \approx 4\pi r^2 t (t << r)$$

Then

$$\frac{v_a}{v_p} = \frac{r}{3t}$$
$$\Rightarrow r \approx 3t\frac{v_a}{v_p} \tag{9}$$

2.5 Results

Figure 5a shows the optimal distribution of two materials corresponding to fibers and parenchyma. The distribution of fibers is comparable to the distribution obtained analytically as well as verified experimentally by Mannan et. al.[16] The variation of parenchyma on the other hand is relatively constant as the cellular material necessary for survival of the cells remains constant while progressively reduces their air content.

(a)   (b)
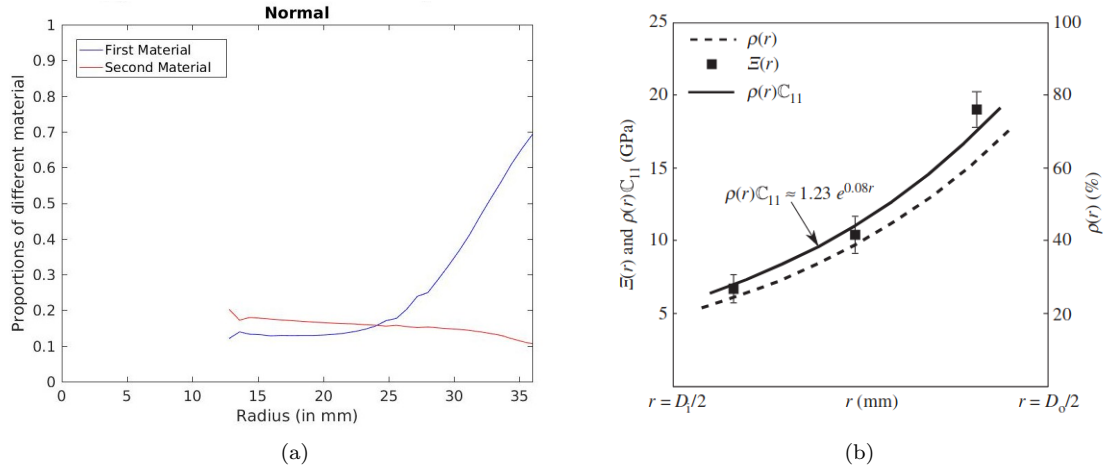
Figure 5: (a)Axisymmetric radial distribution of fibres and parenchyma obtained for an annular rod with inner radius 12mm and outer radius 36mm with $\sigma_{max} = 28$MPa and $M_{max} = 580$ N-m. (b) The variation of areal density $\rho(r)\mathbb{C}$ and the experimental data in dotted line where D_i and D_o are inner and outer diameters respectively. [16]

Figure 6a shows the distribution of fibres for different nodes and fig. 6b shows the same for curved and straight sample. Again both of these look similar to the optimal distribution (fig. 5a).

(a)   (b)
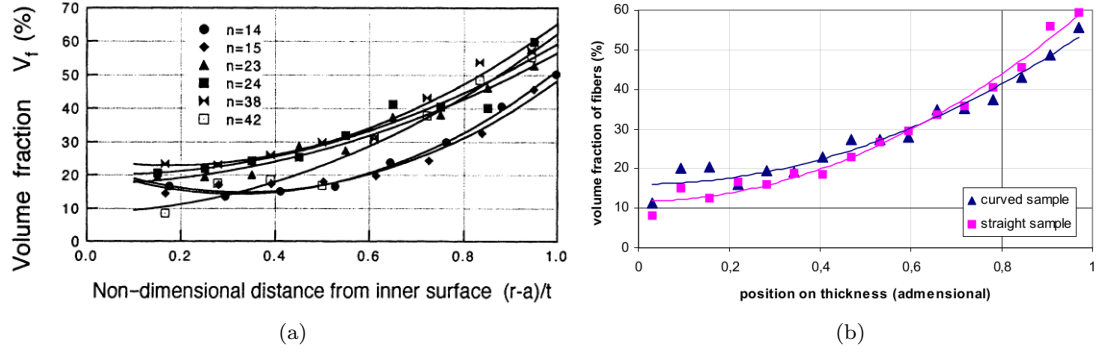
Figure 6: Variation of volume fraction of the fibers with the non-dimensional distance from the inner surface.(a) For different nodes(n), Amada et. al. [1] (b) For different type of samples, Ghavami et. al. [6]
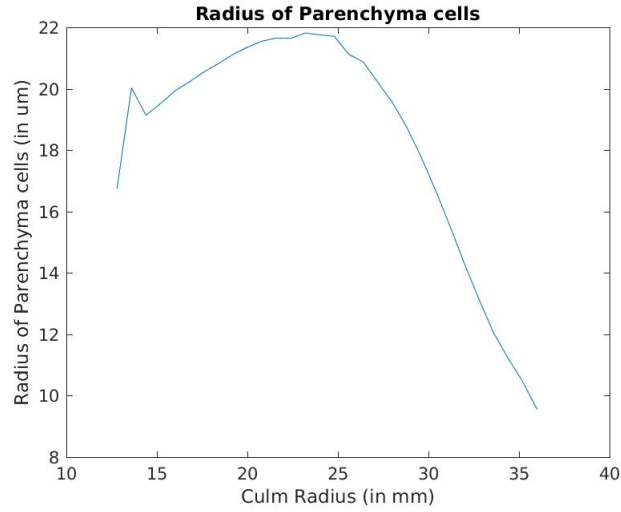
Figure 7: Radius of parenchyma cell size obtained for an annular rod with inner radius 12mm and outer radius 36mm with $\sigma_{max} = 28$MPa and $M_{max} = 580$ N-m

2.5.1 Extreme

We have also obtained results for different types of bamboos, like bamboos with large cross-sectional diameter but thin annular cross-section and bamboos with small diameter but solid cross section with no hollow center.

It should be noted that we didn't have the experimental data for the set of constraint for these cases of bamboos. To obtain these constraints we first provide a rough estimate using the Euler Bernoulli beam equation. Then if the obtained variation of parenchyma cell size goes beyond what is generally observed in nature that set of constraints are rejected and the optimization

8

problem is solved for a new set of sequentially generated constraints. This process is repeated untill a variation of cell size consistent with nature is observed.
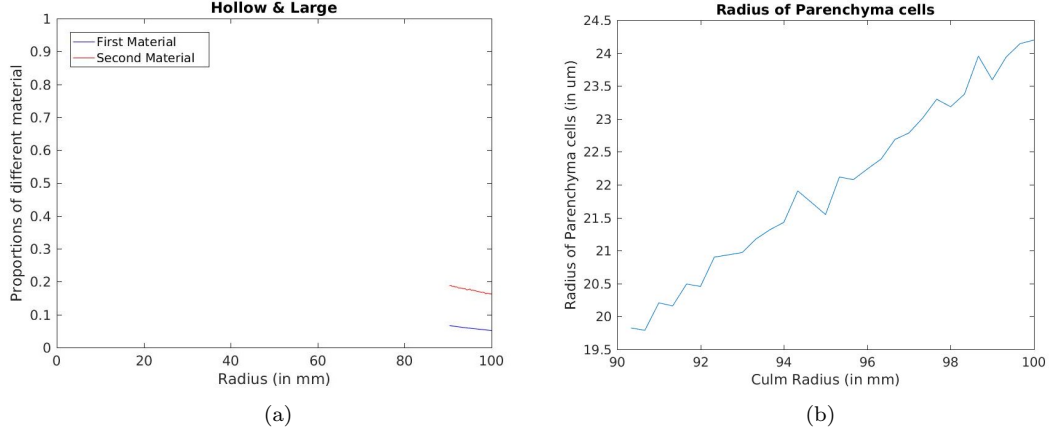
Figure 8: (a)Axisymmetric radial distribution of fibres and parenchyma, (b)Radius of parenchyma cell size obtained for an annular rod with inner radius 90mm and outer radius 100mm with $\sigma_{max} = 150$MPa and $M_{max} = 630$ N-m
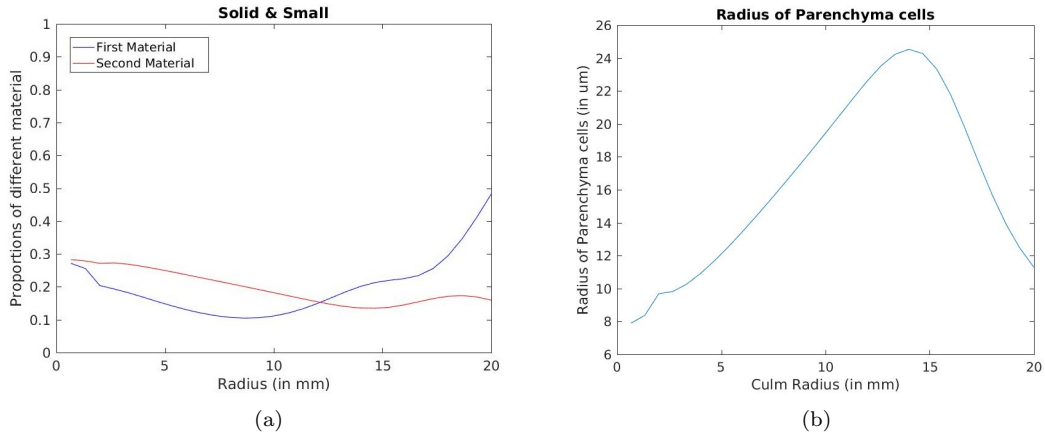
Figure 9: (a)Axisymmetric radial distribution of fibres and parenchyma, (b)Radius of parenchyma cell size obtained for an solid rod with radius 20mm with $\sigma_{max} = 24$MPa and $M_{max} = 420$ N-m

2.5.2 Height

It is assumed that the wind load on the bamboo stem is uniform, as it is similar to a fluid flow over a surface which achieves uniform flow at a height much less than the typical height of the

bamboo. Therefore, the bending moment as a function of height can be expressed as

$$M = Fx = qh\,dh \qquad\qquad\qquad (q \text{ is the uniform loading})$$

$$= \int_h^L qh\,dh = \frac{qh^2}{2}\bigg|_h^L = \frac{qL^2}{2}\left(1 - \frac{h^2}{L^2}\right) = M_{max}\left(1 - \frac{h^2}{L^2}\right)$$

$$(10)$$

where h is the height, q is the uniform loading, L is the total height of the bamboo. L is assumed to be 10m. Similarly, radius of curvature R and stress σ follows

$$R = \frac{EI}{M} = R_0\left(1 - \frac{h^2}{L^2}\right)^{-1} \tag{11}$$

$$\sigma = -\frac{Mr}{I} = \sigma_0\left(1 - \frac{h^2}{L^2}\right) \tag{12}$$

Here R_0 and σ_0 are the minimum radius of curvature and maximum stress which occur at the base of the plant. ¡¿
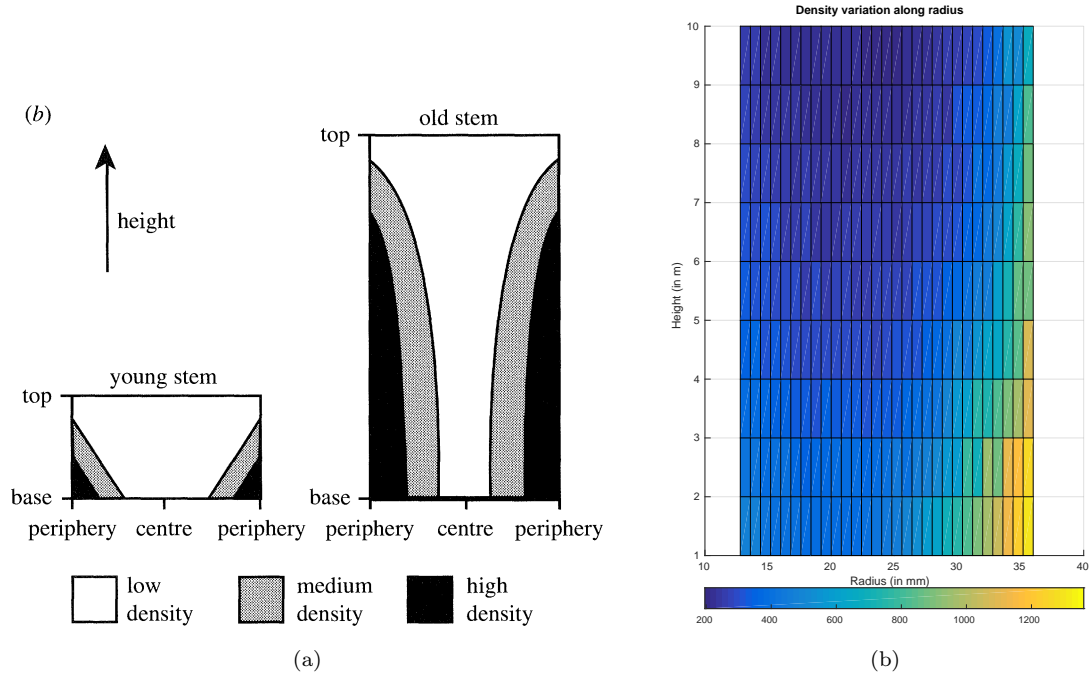
Figure 10: (a) Schematic distribution of material density in young stem (on left) and old plant stem (on right) from Gibson et. al. [7] (b) Density variation with height and radius obtained for an annular rod with inner radius 12mm and outer radius 36mm.

2.6 Conclusion

Comparing with the previous experimentation and studies on bamboo, we can say that the radial distribution of constituent materials of bamboo is optimal for the constraints of maximum stress

10

and bending moment that are applicable to bamboo under the loading conditions. Also, from the results obtained for the variation of material density with height, our results are similar and lies somewhere between a young and an old plant stem.

3 2D Simulation

In the previous chapter, we discussed the optimality of the one-dimensional distribution of the given material of the bamboo for some constraints. To discuss the optimality of the structure originating from this one-dimensional distribution, we will first develop a process for generating optimal structures using topology optimization and finite element methods. Once, we have a sense of what an optimal structure for the given material and loading constraint, we can compare them with the structures found in natural bamboo and be able to comment on its optimality. So, in this chapter, we will discuss the topology optimization of the microstructure for the given constraints on macro-structure.

3.1 Overview

First, an optimization problem is defined for minimizing the overall compliance of the structure with the constraints on volume. For calculating compliance ($\frac{1}{2}F^T U$), at every iteration, we find the displacement U for given force F and other boundary conditions on the macro domain. Displacements are determined by finite element analysis where the stiffness matrix for the macro domain elements is obtained by homogenization method. Each macro domain element is a called base cell and is further meshed to obtain the microstructure. To obtain the homogenized properties, another finite element analysis is done on this microdomain by applying periodic boundary conditions. It is the topology of this structure that we want to optimize. To achieve this, we link the optimality of the objective function to the topology of the microstructure through sensitivity analysis. For each element in the microdomain, a number is determined based on how critical is that element is for minimizing the objective function. After each iteration, the structure is updated based on the sensitivity numbers. This process is repeated until the volume constraint is achieved and the sensitivity numbers converge.
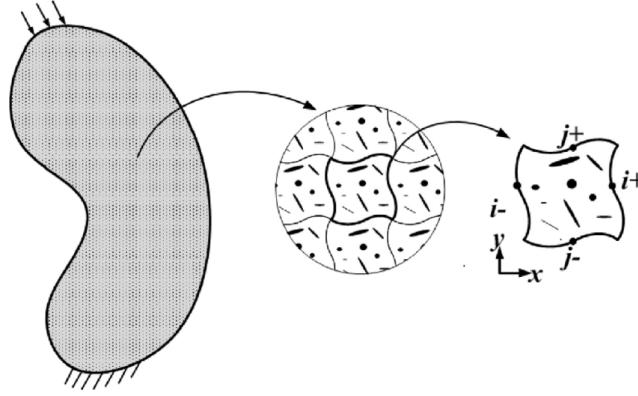
Figure 11: Schematic showing a structure made of periodic microstructure.

3.2 Optimization Problem

$$\begin{aligned} \underset{\chi}{\text{minimize}} : \quad & C = \frac{1}{2}\mathbf{F^T U} \\ \text{subject to:} \quad & \sum_{j=1}^{N} V_j x_j - V_f = 0 \qquad \text{where} \quad x_j = \{0,1\} \end{aligned}$$

(13)

12

Here, $\mathbf{F}$ is the applied load, $\mathbf{U}$ is the displacement of the macrostructure, V_f is the specified volume fraction, V_j is the volume of jth element of the base cell which has a total of N elements. x_j are the design variables represent the relative density. Element is made of material 1 for $x_j = 1$ and material 2 for $x_j = 0$. Figure 12 shows the two sample domains which will be used to test the solution.
[12]
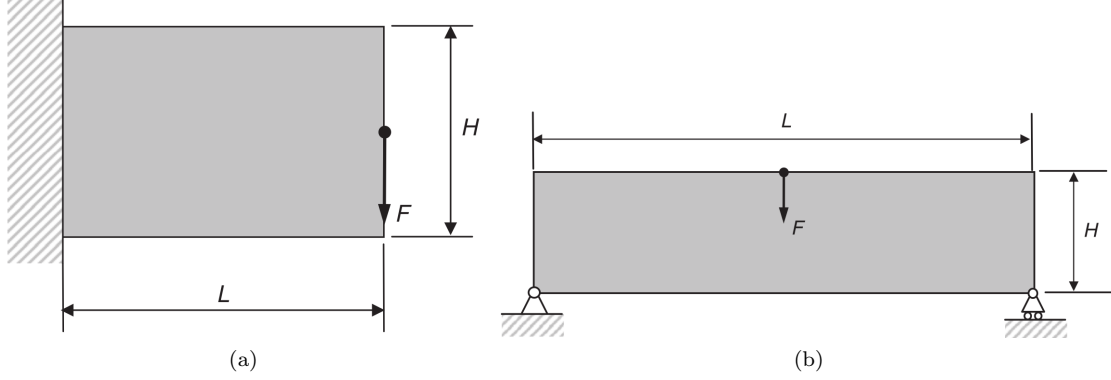
Figure 12: Schematic of (a) cantilever beam and (b) MBB beam

3.3   Finite Element Analysis

The optimization problem defined in (13) requires the finite element analysis to be done on two scales, one for macrostructure and another for the base cell. For the microstructure, since the design variables can be either 0 or 1, Solid Isotropic Material with Penalization model[**?**] is used for obtaining the material properties. Thus, the elasticity matrix can be written as

$$\mathbf{D} = x_j^p \mathbf{D}^1 + (1 - x_j^p)\mathbf{D}^2 \tag{14}$$

where $\mathbf{D}^1$ and $\mathbf{D}^2$ are the elasticity matrices for material 1 and 2 respectively, p is the penalization constant. For the macrodomain, we have the following FE equation

$$\mathbf{KU} = \mathbf{F} \tag{15}$$

where $\mathbf{K}$ is the assembled stiffness matrix for the macrostructure whose each component is calculated using

$$\mathbf{K}_i = \int_{V_i} \mathbf{B}_i^T \mathbf{D}_i^H \mathbf{B}_i dV_i \tag{16}$$

where $\mathbf{B}_i$ is the elemental strain-displacement matrix and $\mathbf{D}_i^H$ is the homogenized elasticity matrix calculated from the finite analysis of the base cell. The homogenization process[**?**] is discussed in the subsequent chapters. In this study, all base cells are assumed to be identical and therefore, equation (16) can be simplified as

$$\mathbf{K}_i = \int_{V_i} \mathbf{B}^T \mathbf{D}^H \mathbf{B} dV_i \tag{17}$$

3.4 Periodic Boundary Conditions

The process of homogenization requires the displacements corresponding to uniform strain fields, i.e., $[\epsilon_{11}, \epsilon_{22}, 2\epsilon_{12}] = [1, 0, 0]^T, [0, 1, 0]^T, [0, 0, 1]^T$. Periodic boundary conditions are needed to solve the finite element problem for uniform strain fields.

If u and v are the components of displacements in p_1 and p_2 directions respectively, then from periodicity, we have

$$
\begin{aligned}
u(p_1, p_2) &= u(p_1 + P_1, p_2) = u(p_1, p_2 + P_2) = u(p_1 + P_1, p_2 + P_2), \\
v(p_1, p_2) &= v(p_1 + P_1, p_2) = v(p_1, p_2 + P_2) = v(p_1 + P_1, p_2 + P_2).
\end{aligned}
\tag{18}
$$

For cases $[1, 0, 0]^T$ and $[0, 1, 0]^T$, from symmetry of loading and geometry w.r.t. q_1, we have

$$
u(p_1, p_2^0) = u(p_1, p_2^0 + P_2), \tag{19}
$$
$$
v(p_1, p_2^0) = -v(p_1, p_2^0 + P_2). \tag{20}
$$

Similarly, using the symmetry about q_2, we have

$$
u(p_1^0, p_2) = -u(p_1^0 + P_1, p_2), \tag{21}
$$
$$
v(p_1^0, p_2) = v(p_1^0 + P_1, p_2). \tag{22}
$$

From eqs (26), (27), and (18), we get

$$
u(p_1^0, p_2) = u(p_1^0 + P_1, p_2) = 0, \tag{23}
$$
$$
v(p_1, p_2^0) = v(p_1, p_2^0 + P_2) = 0. \tag{24}
$$

Eqs (25), (28), (30) and (29) are the required periodic boundary conditions for strain fields $[1, 0, 0]^T$ and $[0, 1, 0]^T$.

Now, For the case of $[0, 0, 1]^T$, loading is anti-symmetric and geometry is symmetric w.r.t. q_1 and q_2, as a result, we have

$$
u(p_1, p_2^0) = -u(p_1, p_2^0 + P_2), \tag{25}
$$
$$
v(p_1, p_2^0) = v(p_1, p_2^0 + P_2). \tag{26}
$$
$$
u(p_1^0, p_2) = u(p_1^0 + P_1, p_2), \tag{27}
$$
$$
v(p_1^0, p_2) = -v(p_1^0 + P_1, p_2). \tag{28}
$$

From eqs (25), (28), and (18), we get

$$
u(p_1, p_2^0) = u(p_1, p_2^0 + P_2) = 0, \tag{29}
$$
$$
v(p_1^0, p_2) = v(p_1^0 + P_1, p_2) = 0. \tag{30}
$$

Eqs (26), (27), (30) and (29) are the required periodic boundary conditions for strain field $[0, 0, 1]^T$.
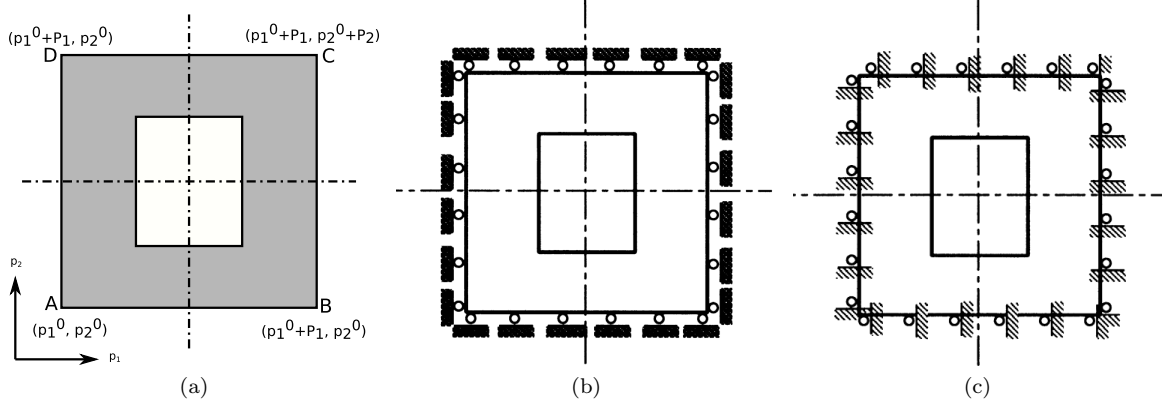
Figure 13: (a)Representative Base cell, (b)PBCs for $[100]^T$ and $[010]^T$ cases, (c)PBCs for $[001]^T$ case

3.4.1 Penalty Method

We have used the penalty method to enforce the above discussed boundary conditions. Let these conditions on the displacements $\{\mathbf{U}\}$ can be written as

$$[\mathbf{C}]\{\mathbf{U}\} = \{\mathbf{Q}\}$$

where $[\mathbf{C}]$ and $\{\mathbf{Q}\}$ are constants. Let us define $\{\mathbf{t}\}$ as

$$\{\mathbf{t}\} = [\mathbf{C}]\{\mathbf{U}\} - \{\mathbf{Q}\}$$

such that $\{\mathbf{t}\} = \{\mathbf{0}\}$ implies that the constraints are satisfied. Any non-negative values of $\{\mathbf{t}\}$ must be penalized to minimize the violation of constraints. This is achieved by augmenting the potential energy function[?] Π with a *penalty function* $\frac{1}{2}\{\mathbf{t}\}^T[\boldsymbol{\alpha}]\{\mathbf{t}\}$, where $[\boldsymbol{\alpha}]$ is a diagonal matrix of penalty numbers. Thus, potential energy function becomes

$$\Pi = \frac{1}{2}\{\mathbf{U}\}^T[\mathbf{K}]\{\mathbf{U}\} - \{\mathbf{U}\}^T\{\mathbf{F}\} + \frac{1}{2}\{\mathbf{t}\}^T[\boldsymbol{\alpha}]\{\mathbf{t}\} \tag{31}$$

where $[\mathbf{K}]$ is the stiffness matrix and $\{\mathbf{F}\}$ are the forces.

For minimum potential energy condition, $\{\frac{\partial \Pi}{\partial \mathbf{U}}\} = \{0\}$, this implies

$$\left([\mathbf{K}] + [\mathbf{C}]^T[\boldsymbol{\alpha}][\mathbf{C}]\right)\{\mathbf{U}\} = \{\mathbf{F}\} + [\mathbf{C}]^T[\boldsymbol{\alpha}]\{\mathbf{Q}\} \tag{32}$$

If $[\boldsymbol{\alpha}]$ is null matrix, all constraints are ignored, else if α_i's are infinite, all constraints are satisfied. For a positive definite $[\mathbf{K}]$, positive penalty numbers are used. We have set all penalty numbers to be same, this means that all constraints are given equal priority, i.e. $[\boldsymbol{\alpha}] = \alpha[I]$. α must be significantly larger to ensure that the constraint violation is negligible. Thus, the eq. (32) reduces to the following

$$\left([\mathbf{K}] + \alpha[\mathbf{C}]^T[\mathbf{C}]\right)\{\mathbf{U}\} = \{\mathbf{F}\} + \alpha[\mathbf{C}]^T\{\mathbf{Q}\} \tag{33}$$

15

Eq (33) has to be solved separately for the three cases of periodic boundary conditions.
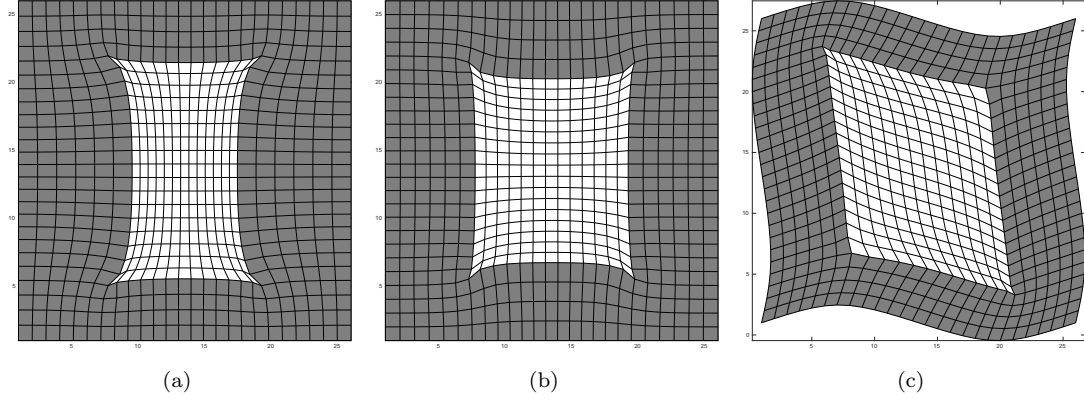
Figure 14: Deformation of the base cell for the strain fields (a) $\epsilon = [1\,0\,0]^T$, (b) $\epsilon = [0\,1\,0]^T$, (c) $\epsilon = [0\,0\,1]^T$

3.5 Homogenization

The homogenization method is generally used to analyze the properties of composites with complex but periodic microstructure. The procedure replaces the composites with an equivalent homogeneous material. The method is based on the two-scale asymptotic expansion of structural responses.

We will now derive the equation for homogenization. Now, the structure is Y-periodic, therefore we have, $E_{ijkl}(\mathbf{y}) = E_{jikl}(\mathbf{y}) = E_{ijlk}(\mathbf{y}) = E_{klij}(\mathbf{y})$ where $\mathbf{y} = \mathbf{x}/\varepsilon$
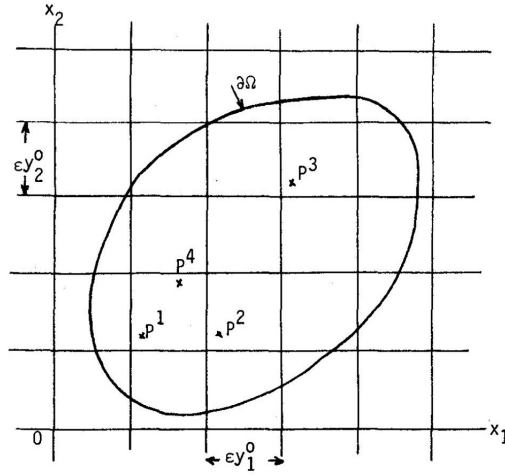
Figure 15: Schematic for periodic structure and double scale modeling

16

$E_{ijkl}(\mathbf{y})$ is assumed to satisfy strong ellipticity condition, i.e., there exists $m > 0$ such that.

$$\sum_{i,j,k,l=1}^{N} E_{ijkl}^{\varepsilon}(x)\mathbf{X}_{ij}\mathbf{X}_{kl} \geq m \sum_{i,j=1}^{N} \mathbf{X}_{ij}\mathbf{X}_{ij} \qquad \forall \quad \mathbf{X}_{ij} = \mathbf{X}_{ji} \tag{34}$$

Let us define

$$E_{ijkl}^{\varepsilon}(\mathbf{x}) = E_{ijkl}(\mathbf{x}, \mathbf{y}), \qquad \mathbf{y} = \frac{\mathbf{x}}{\varepsilon} \tag{35}$$

Let the domain Ω has a boundary Γ. Let $\mathbf{f}$ be the body force acting on Ω and $\mathbf{t}$ be the traction acting on Γ_t part of the boundary Γ. Also, let Γ_D be the part of boundary on which displacement is defined. Then the displacement $\mathbf{u}^{\varepsilon}$ can be obtained as the solution to the following minimization problem

$$\min_{\mathbf{v}^{\varepsilon} \in U} \quad F^{\varepsilon}(\mathbf{v}^{\varepsilon}), \tag{36}$$

where F^{ε} is total potential energy given as

$$F^{\varepsilon}(\mathbf{v}^{\varepsilon}) = \frac{1}{2}\int_{\Omega} E_{ijkl}^{\varepsilon}(\mathbf{x})\epsilon_{kl}(\mathbf{v}^{\varepsilon})\epsilon_{ij}(\mathbf{v}^{\varepsilon})dx - \int_{\Omega} \mathbf{f} \cdot \mathbf{v}^{\varepsilon}dx - \int_{\Gamma_t} \mathbf{t} \cdot \mathbf{v}^{\varepsilon}ds \tag{37}$$

and $\mathcal{U}$ is the set of admissible displacements defined such that

$$\mathcal{U} = \{\mathbf{v} = v_i \mathbf{e}_i : v_i \in H^1(\Omega) \text{ and } \mathbf{v} \in \mathcal{G} \text{ on } \Gamma_D\} \tag{38}$$

where $\mathcal{G}$ is set of displacement defined along the boundary Γ_D.
Let

$$\mathbf{v}^{\varepsilon}(\mathbf{x}) = \mathbf{v}^0(\mathbf{x}) + \varepsilon\mathbf{v}^1(\mathbf{x}, \mathbf{y}), \qquad \mathbf{y} = \frac{\mathbf{x}}{\varepsilon}. \tag{39}$$

Using chain rule for functions in two variables

$$\begin{aligned}
\frac{\partial f(\mathbf{x}, \mathbf{y}(\mathbf{x}))}{\partial \mathbf{x}} &= \frac{\partial f}{\partial \mathbf{x}} + \frac{\partial f}{\partial \mathbf{y}}\frac{\partial \mathbf{y}}{\partial \mathbf{x}} \\
&= \frac{\partial f}{\partial \mathbf{x}} + \frac{1}{\varepsilon}\frac{\partial f}{\partial \mathbf{y}}
\end{aligned} \tag{40}$$

Using above two equations, we can write the linerized strain as

$$\begin{aligned}
\epsilon_{ij}(\mathbf{v}^{\varepsilon}(\mathbf{x})) &= \frac{\partial(v_i^0(\mathbf{x}) + \varepsilon v_i^1(\mathbf{x}, \mathbf{y}))}{\partial x_j} \\
&= \frac{\partial v_i^0}{\partial x_j} + \varepsilon\left\{\frac{\partial v_i^1}{\partial x_j} + \frac{1}{\varepsilon}\frac{\partial v_i^1}{\partial y_j}\right\} \\
&\approx \frac{\partial v_i^0}{\partial x_j} + \frac{\partial v_i^1}{\partial y_j} \qquad\qquad \{\varepsilon \ll 1\}
\end{aligned} \tag{41}$$

Therefore, equation (37) can be written as

$$\begin{aligned}
F^{\varepsilon}(\mathbf{v}^{\varepsilon}) = \frac{1}{2}\int_{\Omega} E_{ijkl}^{\varepsilon}(\mathbf{x})\left(\frac{\partial v_k^0}{\partial x_l} + \frac{\partial v_k^1}{\partial y_l}\right)\left(\frac{\partial v_i^0}{\partial x_j} + \frac{\partial v_i^1}{\partial y_j}\right)dx \\
- \int_{\Omega} \mathbf{f} \cdot \mathbf{v}^0 dx - \int_{\Gamma_t} \mathbf{t} \cdot \mathbf{v}^0 ds + \varepsilon R^{\varepsilon}(\mathbf{v}^0, \mathbf{v}^1) \quad (42)
\end{aligned}$$

17

Here, R^ε is the contribution of $\varepsilon \mathbf{v}^1$ in the calculation of energy from body force and traction. Using average operator

$$\Phi^\varepsilon(\mathbf{x}) = \frac{1}{|Y|} \int_Y \Phi(\mathbf{x}, \mathbf{y}) dy, \tag{43}$$

we get,

$$
\begin{aligned}
F^\varepsilon(\mathbf{v}^\varepsilon) &= F(\mathbf{v}^0, \mathbf{v}^1) \\
&= \frac{1}{2|Y|} \int_\Omega \int_Y E_{ijkl}(\mathbf{x}, \mathbf{y}) \left(\frac{\partial v_k^0}{\partial x_l} + \frac{\partial v_k^1}{\partial y_l} \right) \left(\frac{\partial v_i^0}{\partial x_j} + \frac{\partial v_i^1}{\partial y_j} \right) dy\, dx \\
&\quad - \int_\Omega \mathbf{f} \cdot \mathbf{v}^0 dx - \int_{\Gamma_t} \mathbf{t} \cdot \mathbf{v}^0 ds
\end{aligned}
\tag{44}
$$

Let $\mathbf{u}^\varepsilon \{\mathbf{u}^0, \mathbf{u}_1\}$ be a minimizer of the functional F, then

$$\frac{1}{|Y|} \int_\Omega \int_Y E_{ijkl}(x,y) \left(\frac{\partial u_k^0}{\partial x_l} + \frac{\partial u_k^1}{\partial y_l} \right) \left(\frac{\partial v_i^0}{\partial x_j} \right) dy\, dx = \int_\Omega \mathbf{f} \cdot \mathbf{v}^0 dx + \int_{\Gamma_t} \mathbf{t} \cdot \mathbf{v}^0 ds \quad \forall \mathbf{v}^0 \tag{45}$$

$$\frac{1}{|Y|} \int_\Omega \int_Y E_{ijkl}(x,y) \left(\frac{\partial u_k^0}{\partial x_l} + \frac{\partial u_k^1}{\partial y_l} \right) \left(\frac{\partial v_i^1}{\partial x_j} \right) dy\, dx = 0, \quad \forall \mathbf{v}^1 \tag{46}$$

Let u_k^1 be a function of directional derivative of u^0 times the displacement of the base cell element in that direction. Here χ is the microscopic displacement field which satisfies the condition of Y-periodicity.

$$u_k^1(x, y) = -\chi_k^{pq}(y) \frac{\partial u_p^0}{\partial x_q}(x), \tag{47}$$

Then, eq (46) becomes

$$\int_\Omega \frac{\partial u_k^0}{\partial x_l} dx \cdot \int_Y \left(E_{ijkl} - E_{ijpq} \frac{\partial \chi_p^{kl}}{\partial y_q} \right) \frac{\partial v_i^1}{\partial x_j} dy = 0 \tag{48}$$

$$\Rightarrow \int_Y \left(E_{ijkl} - E_{ijpq} \frac{\partial \chi_p^{kl}}{\partial y_q} \right) \frac{\partial v_i^1}{\partial x_j} dy = 0 \qquad \text{for k, l = 1 and 2,} \tag{49}$$

Similarly, substituting equation (47) in (45) gives the homogenized equation.

$$
\begin{aligned}
\text{LHS} &= \frac{1}{|Y|} \int_\Omega \int_Y E_{ijkl}(x,y) \left(\frac{\partial u_k^0}{\partial x_l} + \frac{\partial u_k^1}{\partial y_l} \right) \left(\frac{\partial v_i^0}{\partial x_j} \right) dy\, dx \\
&= \frac{1}{|Y|} \int_\Omega \int_Y \left(E_{ijkl} \frac{\partial u_k^0}{\partial x_l} - E_{ijpq} \frac{\partial \chi_p^{kl}}{\partial y_q} \frac{\partial u_k^0}{\partial x_l} \right) \frac{\partial v_i^0}{\partial x_j} dy\, dx \\
&= \frac{1}{|Y|} \int_\Omega \left\{ \int_Y \left(E_{ijkl} - E_{ijpq} \frac{\partial \chi_p^{kl}}{\partial y_q} \right) dy \right\} \frac{\partial u_k^0}{\partial x_l} \frac{\partial v_i^0}{\partial x_j} dx \\
&= \int_\Omega E_{ijkl}^H(x) \frac{\partial u_k^0}{\partial x_l} \frac{\partial v_i^0}{\partial x_j} dx
\end{aligned}
$$

Homogenized equation

$$\int_\Omega E_{ijkl}^H(x) \frac{\partial u_k^0}{\partial x_l} \frac{\partial v_i^0}{\partial x_j} dx = \int_\Omega \mathbf{f} \cdot \mathbf{v}^0 dx + \int_{\Gamma_t} \mathbf{t} \cdot \mathbf{v}^0 ds \qquad \text{for every } \mathbf{v}^0 \tag{50}$$

18

where $E_{ijkl}^H(x)$ is

$$\boxed{E_{ijkl}^H = \frac{1}{|Y|} \int_Y \left(E_{ijkl} - E_{ijpq} \frac{\partial \chi_p^{kl}}{\partial y_q} \right) dy} \tag{51}$$

3.5.1 Implementation

For 2D problems, it is sufficient to solve (51) for $i, j, p, q = \{1, 2\}$ and three cases for $\{k, l\} = \{1, 1\}, \{2, 2\}, \{1, 2\}$. In this section, we will refer $\mathbf{v}^1$ as $\mathbf{v}$. Assuming orthotropicity, we solve eq (49) for $\{k, l\} = \{1, 1\}$ we get

$$\begin{aligned}
\int_Y &\left\{ \left(E_{1111} \frac{\partial \chi_1^{11}}{\partial y_1} + E_{1122} \frac{\partial \chi_2^{11}}{\partial y_2} \right) \frac{\partial v_1}{\partial y_1} + E_{1212} \left(\frac{\partial \chi_1^{11}}{\partial y_2} + \frac{\partial \chi_2^{11}}{\partial y_1} \right) \left(\frac{\partial v_1}{\partial y_2} + \frac{\partial v_2}{\partial y_1} \right) \right. \\
&\left. + \left(E_{2211} \frac{\partial \chi_1^{11}}{\partial y_1} + E_{2222} \frac{\partial \chi_2^{11}}{\partial y_2} \right) \frac{\partial v_2}{\partial y_2} \right\} dy = \int_Y \left(E_{1111} \frac{\partial v_1}{\partial y_1} + E_{2211} \frac{\partial v_2}{\partial y_2} \right) dy
\end{aligned} \tag{52}$$

From equations (51) and (52), we have

$$E_{1111}^H = \frac{1}{|Y|} \int_Y \left(E_{1111} - E_{1111} \frac{\partial \chi_1^{11}}{\partial y_1} - E_{1122} \frac{\partial \chi_2^{11}}{\partial y_2} \right) dy \tag{53}$$

$$E_{2211}^H = \frac{1}{|Y|} \int_Y \left(E_{2211} - E_{2211} \frac{\partial \chi_1^{11}}{\partial y_1} - E_{2222} \frac{\partial \chi_2^{11}}{\partial y_2} \right) dy \tag{54}$$

Let $\chi^{11} = \hat{\mathbf{u}}^1, \chi^{22} = \hat{u}^2, \chi^{12} = \hat{u}^3$ and $E_{1111} = D_{11}, E_{2222} = D_{22}, E_{1212} = D_{66}, E_{1122} = E_{2211} = D_{12}$. Then eq (52) becomes

$$\begin{aligned}
\int_Y &\left\{ \left(D_{11} \frac{\partial \hat{u}_1^1}{\partial y_1} + D_{12} \frac{\partial \hat{u}_2^1}{\partial y_2} \right) \frac{\partial v_1}{\partial y_1} + D_{66} \left(\frac{\partial \hat{u}_1^1}{\partial y_2} + \frac{\partial \hat{u}_2^1}{\partial y_1} \right) \left(\frac{\partial v_1}{\partial y_2} + \frac{\partial v_2}{\partial y_1} \right) \right. \\
&\left. + \left(D_{12} \frac{\partial \hat{u}_1^1}{\partial y_1} + D_{22} \frac{\partial \hat{u}_2^1}{\partial y_2} \right) \frac{\partial v_2}{\partial y_2} \right\} dy = \int_Y \left(D_{11} \frac{\partial v_1}{\partial y_1} + D_{12} \frac{\partial v_2}{\partial y_2} \right) dy
\end{aligned} \tag{55}$$

and eq (53) becomes

$$D_{11}^H = \frac{1}{|Y|} \int_Y \left(D_{11} - D_{11} \frac{\partial \hat{u}_1^1}{\partial y_1} - D_{12} \frac{\partial \hat{u}_2^1}{\partial y_2} \right) dy \tag{56}$$

Rearranging Eq. (55)

$$\begin{aligned}
\int_Y &\left\{ \frac{\partial v_1}{\partial y_1} \quad \frac{\partial v_2}{\partial y_2} \quad \frac{\partial v_1}{\partial y_2} + \frac{\partial v_2}{\partial y_1} \right\} \begin{bmatrix} D_{11} & D_{12} & 0 \\ D_{12} & D_{22} & 0 \\ 0 & 0 & D_{66} \end{bmatrix} \times \begin{bmatrix} \frac{\partial \hat{u}_1^1}{\partial y_1} \\ \frac{\partial \hat{u}_2^1}{\partial y_2} \\ \frac{\partial \hat{u}_1^1}{\partial y_2} + \frac{\partial \hat{u}_2^1}{\partial y_1} \end{bmatrix} dY \\
&= \int_Y \left\{ \frac{\partial v_1}{\partial y_1} \quad \frac{\partial v_2}{\partial y_2} \quad \frac{\partial v_1}{\partial y_2} + \frac{\partial v_2}{\partial y_1} \right\} \begin{bmatrix} D_{11} \\ D_{12} \\ 0 \end{bmatrix} dY
\end{aligned} \tag{57}$$

Let us define

$$\mathbf{b} = \begin{bmatrix} \frac{\partial}{\partial y_1} & 0 \\ 0 & \frac{\partial}{\partial y_2} \\ \frac{\partial}{\partial y_1} & \frac{\partial}{\partial y_2} \end{bmatrix} \tag{58}$$

19

and

$$\mathbf{D} = \begin{bmatrix} \mathbf{d}_1 & \mathbf{d}_2 & \mathbf{d}_3 \end{bmatrix} \tag{59}$$

Then Eq (57), can be written as

$$\int_Y \mathbf{v}^T \mathbf{b}^T \mathbf{D} \mathbf{b} \hat{\mathbf{u}}^1 \, dY = \int_Y \mathbf{v}^T \mathbf{b}^T \mathbf{d}_1 \qquad \forall \mathbf{v} \in \mathbf{V}_Y \tag{60}$$

and eq. (56) becomes:

$$\boxed{D_{11}^H = \frac{1}{|Y|} \int_Y \left(D_{11} - \mathbf{d}_1^T \mathbf{b} \hat{\mathbf{u}}^1 \right) dy} \tag{61}$$

Similarly, we can derive

$$D_{12}^H = \frac{1}{|Y|} \int_Y \left(D_{12} - \mathbf{d}_1^T \mathbf{b} \hat{\mathbf{u}}^2 \right) dy \tag{62}$$

$$D_{22}^H = \frac{1}{|Y|} \int_Y \left(D_{22} - \mathbf{d}_2^T \mathbf{b} \hat{\mathbf{u}}^2 \right) dy \tag{63}$$

$$D_{66}^H = \frac{1}{|Y|} \int_Y \left(D_{66} - \mathbf{d}_3^T \mathbf{b} \hat{\mathbf{u}}^3 \right) dy \tag{64}$$

Assembling $\mathbf{D}^H$ from eqs (61)-(64)

$$\boxed{\mathbf{D}^H = \frac{1}{|Y|} \int_Y \mathbf{D} \left(\mathbf{I} - \mathbf{b} \hat{\mathbf{u}} \right) dy} \tag{65}$$

Here, the microscopic displacements are determined by applying periodic boundary conditions as explained in previous section.

3.6   Sensitivity Analysis

Sensitivity analysis of the objective function is necessary for linking the topology of the base cell to the compliance of the structure. From eq (13), we can write the compliance of one material unit cell as

$$C_i = \frac{1}{2} \mathbf{U}_i^T \mathbf{K}_i^T \mathbf{U}_i = \frac{1}{2} \mathbf{U}_i^T \mathbf{K}_i \mathbf{U}_i \tag{66}$$

Now, the macrostructure is composed of identical base cell. Therefore, the sensitivity of the compliance complete structure w.r.t the relative densities(the design variables) of microstructure will be the average of sensitivities of compliance of all the macrostructure elements w.r.t. the base cell design variable. i.e.,

$$\begin{aligned}
\frac{dC}{dx_j} &= \frac{1}{2M} \sum_{i=1}^M \mathbf{U}_i^T \frac{\partial \mathbf{K}_i}{\partial x_j} \mathbf{U}_i \\
&= \frac{1}{2M} \sum_{i=1}^M \mathbf{U}_i^T \int_{V_i} \mathbf{B}^T \frac{\partial \mathbf{D}^H}{\partial x_j} \mathbf{B} dV_i \, \mathbf{U}_i
\end{aligned} \tag{67}$$

here M is total number of elements in the macrostructure. From eq (65), we can write

$$\frac{\partial \mathbf{D}^H}{\partial x_j} = \frac{1}{|Y|} \int_Y \left(\mathbf{I} - \mathbf{b}\hat{\mathbf{u}}\right)^T \frac{\partial \mathbf{D}}{\partial x_j} \left(\mathbf{I} - \mathbf{b}\hat{\mathbf{u}}\right) dy \tag{68}$$

Using eq (14)

$$\frac{\partial \mathbf{D}^H}{\partial x_j} = \frac{p x_j^{p-1}}{|Y_j|} \int_{Y_j} \left(\mathbf{I} - \mathbf{b}\hat{\mathbf{u}}_j\right)^T (\mathbf{D}^1 - \mathbf{D}^2)\left(\mathbf{I} - \mathbf{b}\hat{\mathbf{u}}_j\right) dy_j \tag{69}$$

Now, eq (67) becomes

$$\frac{dC}{dx_j} = \frac{p x_j^{p-1}}{2M|Y_j|} \sum_{i=1}^{M} \mathbf{U}_i^T \left(\int_{V_i} \mathbf{B}^T \left[\int_{Y_j} \left(\mathbf{I} - \mathbf{b}\hat{\mathbf{u}}_j\right)^T (\mathbf{D}^1 - \mathbf{D}^2)\left(\mathbf{I} - \mathbf{b}\hat{\mathbf{u}}_j\right) dy_j \right] \mathbf{B} dV_i \right) \mathbf{U}_i \tag{70}$$

Therefore, the elemental sensitivity numbers can be defined as

$$\begin{aligned}
\alpha_j &= \frac{2M}{p} \frac{dC}{dx_j} \\
&= \frac{x_j^{p-1}}{|Y_j|} \sum_{i=1}^{M} \mathbf{U}_i^T \left(\int_{V_i} \mathbf{B}^T \left[\int_{Y_j} \left(\mathbf{I} - \mathbf{b}\hat{\mathbf{u}}_j\right)^T (\mathbf{D}^1 - \mathbf{D}^2)\left(\mathbf{I} - \mathbf{b}\hat{\mathbf{u}}_j\right) dy_j \right] \mathbf{B} dV_i \right) \mathbf{U}_i
\end{aligned} \tag{71}$$

Here, both M and p are constant for the problem. Also, if the elements of the base cell are identical $|Y|_j$ term can also be removed. Since, we are doing a discrete optimization meaning x_j's can only be 0 or 1, at every iteration we set elements with high sensitivities to 1 and others to 0.

3.7 Fitering

Topology optimization techniques often faces problems such as numerical instability consequences. These instabilities leads to checkerboard pattern in the topology, mesh dependency of the solution etc. To get rid off such problem, the technique of filtering is used. There are many filter that are being used in topology optimization problems. We have used a weighted mean sensitivity filter. The modified sensitivity numbers are

$$\hat{\alpha}_j = \frac{\sum_{k=1}^{N} w(r_{jk}) \alpha_k}{\sum_{k=1}^{N} w(r_{jk})} \tag{72}$$

where r_{jk} is the euclidean distance between jth and kth element in the base cell. $w(r_{jk})$ is the weight assigned to the sensitivity number of kth element.

$$w(r_{jk}) = \begin{cases} r_0 - r_{jk} & ; r_{jk} < r_0 \\ 0 & ; r_{jk} \geq r_0 \end{cases} \tag{73}$$

where r_0 is the filter radius. Further, to get gradual improvement in the topology, an average is taken with the sensitivity numbers from the previous iteration, i.e.,

$$\hat{\alpha}_j^t = \frac{1}{2}(\hat{\alpha}_j^{t-1} + \hat{\alpha}_j^t) \tag{74}$$

3.8 Procedure

The complete procedure for optimization is as follows

Step 1: Initialise the design variables x_js, set parameters: filtering radius r_0, delta δ. Define material properties, elasticity matrices $\mathbf{D}$ and densities ρ.

Step 2: Find microscopic displacement field $\hat{\mathbf{u}}$ using finite element analysis by applying periodic boundary conditions.

Step 3: Find the homogenized elasticity matrix of the base cell by plugging the microscopic displacement field in (65).

Step 4: Determine the macroscopic displacement $\mathbf{U}$ through finite element analysis using homogenized material properties $\mathbf{D}^H$. Calculate compliance C of structure using eq (13).

Step 5: Do the sensitivity analysis to find sensitivity numbers α_js

Step 6: Apply the weighted mean filter to obtain filtered sensitivity numbers $\hat{\alpha}_j$s

Step 7: Determine the volume target for the current iteration as following

$$V_f^t = \begin{cases} V_f^{t-1}(1-\delta); & V_f^{t-1} > V_f \text{ and } V_f^{t-1}(1-\delta) \leq V_f \\ V_f^{t-1}(1+\delta); & V_f^{t-1} < V_f \text{ and } V_f^{t-1}(1+\delta) \geq V_f \\ V_f; & otherwise \end{cases} \tag{75}$$

Step 8: Sort the filtered sensitivity numbers and set the design variable x_js corresponding to the top NV_f^t sensitivity numbers to 1 and the other to 0.

Step 9: Repeat steps 2 to 8 until the target volume is reached and the convergence criteria is met. In this thesis we have taken the determinant of sensitivity number matrix as the convergence criteria.
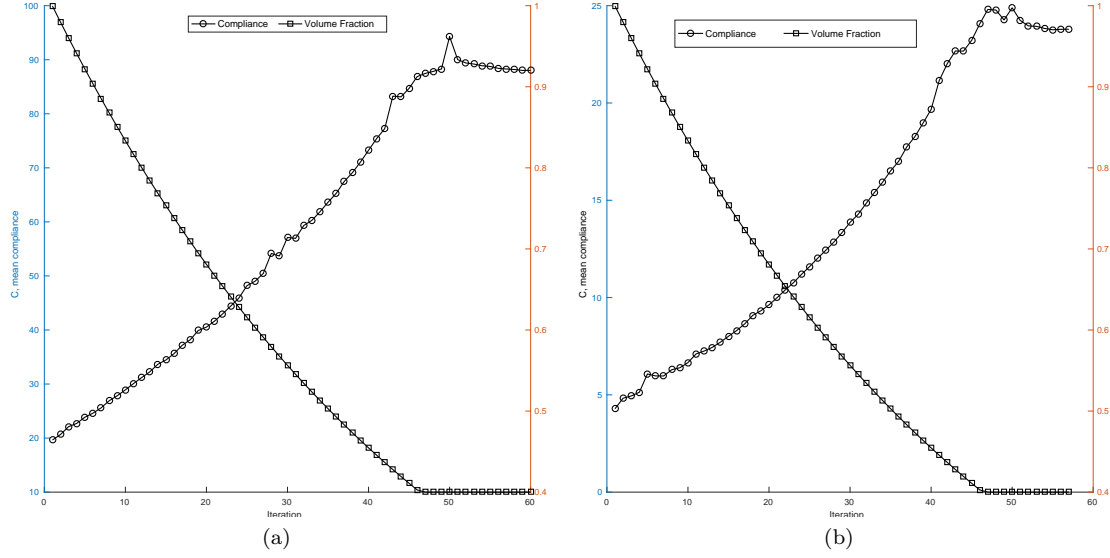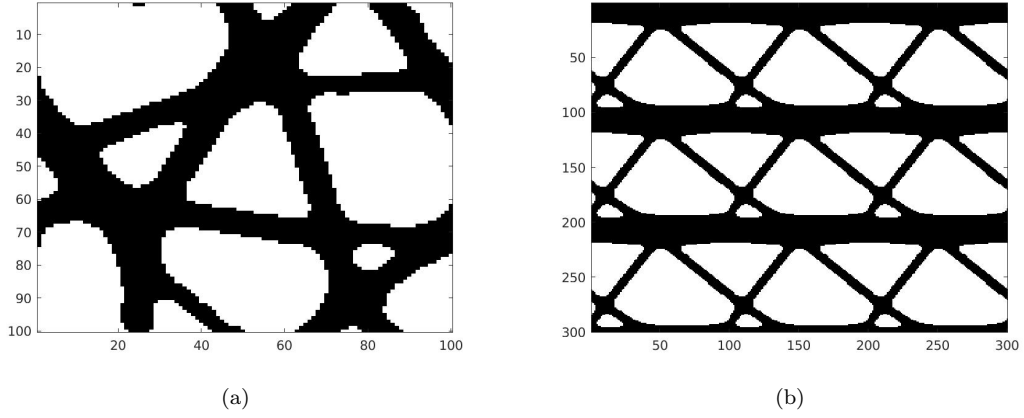
3.9 Results

Figure 16: Evolution of structure (a) Cantilever beam (40x20) (b) MBB beam (40x20)

$$D^H = \begin{bmatrix} 0.3052 & 0.0487 & 0 \\ 0.0487 & 0.0927 & 0 \\ 0 & 0 & 0.0504 \end{bmatrix}$$

(c)

Figure 17: (a) Optimized base cell, (b) 3x3 arrangement of base cell, (c) D^H matrix of the base cell for Cantilever beam of L=40, H=20 starting with design 1

(a)

(b)

$$D^H = \begin{bmatrix} 0.1938 & 0.0869 & 0 \\ 0.0869 & 0.2239 & 0 \\ 0 & 0 & 0.0943 \end{bmatrix}$$

(c)

Figure 18: (a) Optimized base cell, (b) 3x3 arrangement of base cell, (c) D^H matrix of the base cell for Cantilever beam of L=20, H=40 starting with design 1

(a)

(b)

$$D^H = \begin{bmatrix} 0.1938 & 0.0869 & 0 \\ 0.0869 & 0.2239 & 0 \\ 0 & 0 & 0.0943 \end{bmatrix}$$

(c)

Figure 19: (a) Optimized base cell, (b) 3x3 arrangement of base cell, (c) D^H matrix of the base cell for Cantilever beam of L=20, H=40 starting with design 1
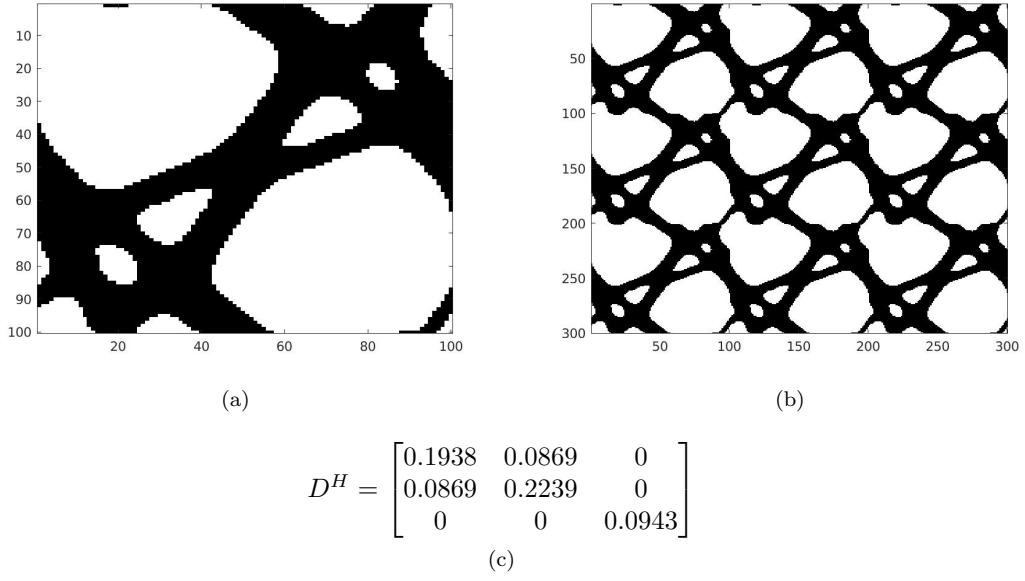
(a)

(b)

$$D^H = \begin{bmatrix} 0.1871 & 0.0620 & 0.0011 \\ 0.0620 & 0.2220 & 0.0124 \\ 0.0011 & 0.0124 & 0.0660 \end{bmatrix}$$

(c)

Figure 20: (a) Optimized base cell, (b) 3x3 arrangement of base cell, (c) D^H matrix of the base cell for MBB beam of L=40, H=20 starting with design 1

(a)

(b)

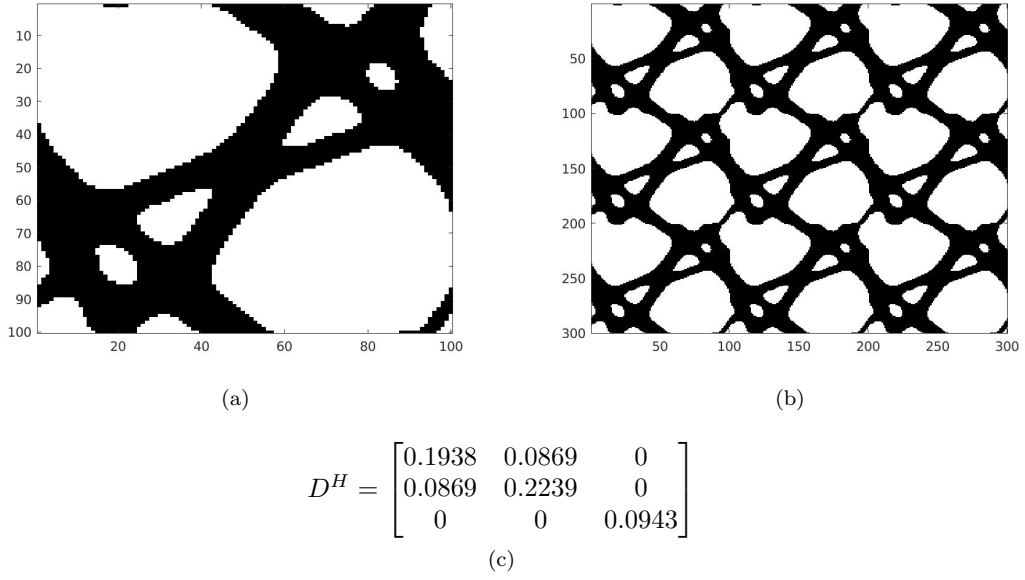$$D^H = \begin{bmatrix} 0.3273 & 0.0477 & 0 \\ 0.0477 & 0.0547 & 0 \\ 0 & 0 & 0.0608 \end{bmatrix}$$

Figure 21: (a) Optimized base cell, (b) 3x3 arrangement of base cell, (c) D^H matrix of the base cell for Cantilever beam of L=40, H=20 starting with design 2
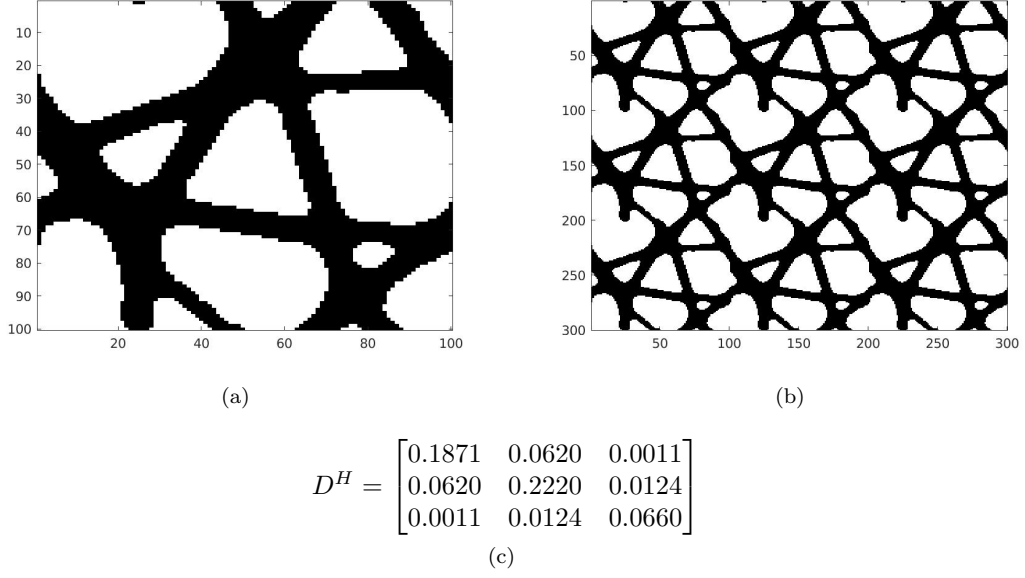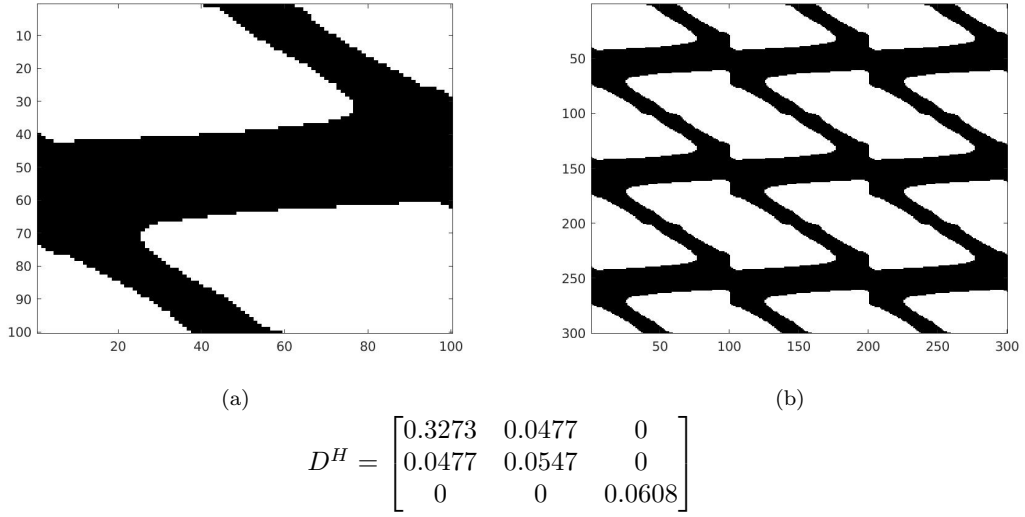
25

References

[1] Shigeyasu Amada, Tamotsu Munekata, Yukito Nagase, Yoshinobu Ichikawa, Atsushi Kirigai, and Yang Zhifei. The mechanical structures of bamboos in viewpoint of functionally gradient and composite materials. *Journal of Composite Materials*, 30(7):800–819, 1996.

[2] Michael Farries Ashby, LJ Gibson, U Wegst, and R Olive. The mechanical properties of natural materials. i. material property charts. *Proceedings of the Royal Society of London. Series A: Mathematical and Physical Sciences*, 450(1938):123–140, 1995.

[3] Martin P Bendsøe. *Topology optimization.* Springer, 2009.

[4] Martin Philip Bendsøe and Noboru Kikuchi. Generating optimal topologies in structural design using a homogenization method. *Computer methods in applied mechanics and engineering*, 71(2):197–224, 1988.

[5] Suresh Bhalla, Supratic Gupta, Puttagunta Sudhakar, and Rupali Suresh. Bamboo as green alternative to concrete and steel for modern structures. *J. Environ. Res. Dev*, 3(2), 2008.

[6] K Ghavami, C de S Rodrigues, and S Paciornik. Bamboo: functionally graded composite material. 2003.

[7] Lorna J Gibson, Michael Farries Ashby, GN Karam, U Wegst, and HR Shercliff. The mechanical properties of natural materials. ii. microstructures for mechanical efficiency. *Proceedings of the Royal Society of London. Series A: Mathematical and Physical Sciences*, 450(1938):141–162, 1995.

[8] Dietger Grosser and Walter Liese. On the anatomy of asian bamboos, with special reference to their vascular bundles. *Wood Science and technology*, 5(4):290–312, 1971.

[9] Meisam K Habibi, Arash T Samaei, Behnam Gheshlaghi, Jian Lu, and Yang Lu. Asymmetric flexural behavior from bamboos functionally graded hierarchical structure: underlying mechanisms. *Acta biomaterialia*, 16:178–186, 2015.

[10] Behrooz Hassani and E Hinton. A review of homogenization and topology opimization iianalytical and numerical solution of homogenization equations. *Computers & structures*, 69(6):719–738, 1998.

[11] X Huang, A Radman, and YM Xie. Topological design of microstructures of cellular materials for maximum bulk or shear modulus. *Computational Materials Science*, 50(6):1861–1870, 2011.

[12] X Huang, SW Zhou, YM Xie, and Q Li. Topology optimization of microstructures of cellular materials and composites for macrostructures. *Computational Materials Science*, 67:397–407, 2013.

[13] Xiaodong Huang, Shiwei Zhou, Guangyong Sun, Guangyao Li, and Yi Min Xie. Topology optimization for microstructures of viscoelastic composite materials. *Computer Methods in Applied Mechanics and Engineering*, 283:503–516, 2015.

[14] Boyan Stefanov Lazarov and Ole Sigmund. Filters in topology optimization based on helmholtz-type differential equations. *International Journal for Numerical Methods in Engineering*, 86(6):765–781, 2011.

[15] Sayyad Mannan, Venkitanarayanan Parameswaran, and Sumit Basu. Stiffness and toughness gradation of bamboo from a damage tolerance perspective. *International Journal of Solids and Structures*, 143:274–286, 2018.

[16] Sayyad Mannan, J Paul Knox, and Sumit Basu. Correlations between axial stiffness and microstructure of a species of bamboo. *Royal Society open science*, 4(1):160412, 2017.

[17] L Mwaikambo. Review of the history, properties and application of plant fibres. *African Journal of Science and Technology*, 7(2):121, 2006.

[18] Bin Niu, Jun Yan, and Gengdong Cheng. Optimum structure with homogeneous optimum cellular material for maximum fundamental frequency. *Structural and Multidisciplinary Optimization*, 39(2):115, 2009.

[19] Fumio Nogata and Hideaki Takahashi. Intelligent functionally graded material: bamboo. *Composites Engineering*, 5(7):743–751, 1995.

[20] G Papanicolau, A Bensoussan, and J-L Lions. *Asymptotic analysis for periodic structures*, volume 5. Elsevier, 1978.

[21] Enrique Sánchez-Palencia. Non-homogeneous media and vibration theory. *Lecture notes in physics*, 127, 1980.

[22] Ole Sigmund and Joakim Petersson. Numerical instabilities in topology optimization: a survey on procedures dealing with checkerboards, mesh-dependencies and local minima. *Structural optimization*, 16(1):68–75, 1998.

[23] Emílio Carlos Nelli Silva, Matthew C Walters, and Glaucio H Paulino. Modeling bamboo as a functionally graded material: lessons for the analysis of affordable materials. *Journal of Materials Science*, 41(21):6991–7004, 2006.

[24] Krister Svanberg. Mma and gcmma-two methods for nonlinear optimization. *vol*, 1:1–15, 2007.

[25] Ulrike GK Wegst, Hao Bai, Eduardo Saiz, Antoni P Tomsia, and Robert O Ritchie. Bioinspired structural materials. *Nature materials*, 14(1):23, 2015.

[26] Sina Youssefian and Nima Rahbar. Molecular origin of strength and stiffness in bamboo fibrils. *Scientific reports*, 5:11116, 2015.

[27] Weihong Zhang and Shiping Sun. Scale-related topology optimization of cellular materials and structures. *International Journal for numerical methods in Engineering*, 68(9):993–1011, 2006.